Biogeosciences Discuss., 8, 1483–1527, 2011
www.biogeosciences-discuss.net/8/1483/2011/
doi:10.5194/bgd-8-1483-2011

Biogeosciences Discussions

Mega fire emissions in Siberia: potential supply of soluble iron from forests to the ocean

A. Ito

Research Institute for Global Change, JAMSTEC, Yokohama, Kanagawa, 236–0001, Japan

Received: 10 December 2010 – Accepted: 9 February 2011 – Published: 18 February 2011

Correspondence to: A. Ito (akinorii@jamstec.go.jp)

Published by Copernicus Publications on behalf of the European Geosciences Union.

Abstract

Significant amounts of carbon and nutrients are released to the atmosphere due to large fires in forests. Characterization of the spatial distribution and temporal variation of the intense fire emissions is crucial for assessing the atmospheric loadings of aerosols and trace gases. This paper discusses issues of the representation of forest fires in the estimation of emissions and the application to an atmospheric chemistry transport model (CTM). The potential contribution of forest fires to the deposition of soluble iron (Fe) into the ocean is highlighted, with a focus on mega fires in eastern Siberia. Satellite products of burned area, active fire, and land cover are used to estimate biomass burning emissions in conjunction with a biogeochemical model. Satellite-derived plume height from MISR is used for the injection height of boreal forest fire emissions. This methodology is applied to quantify fire emission rates in each three-dimensional grid location in the high latitude Northern Hemisphere (> 30° N latitude) over a 5-year period from 2001 to 2005. There is large interannual variation in forest burned area during 2001–2005 (13–51 × 10^3 km^2 yr^{-1}) which results in a corresponding variation in the annual emissions of carbon monoxide (CO) (12–78 Tg CO yr^{-1}). Satellite observations of CO from MOPITT are used to evaluate the model performance in simulating the spatial distribution and temporal variation of the fire emissions. During the major Siberian fire seasons in the summer of 2002 and in the spring of 2003, the model results for CO enhancements due to intense fires are in good agreement with MOPITT observations. These fire emission rates are applied to the aerosol chemistry transport model to examine the relative importance of biomass burning sources of soluble iron compared to those from dust sources. Compared to the dust sources without the atmospheric processing by acidic species, extreme fire events contribute to a significant deposition of soluble iron (10–60%) to downwind regions over the western North Pacific Ocean. It may imply that the supply of nutrients from large forest fires plays a role as a negative biosphere-climate feedback with regards to the ocean fertilization.

BGD
8, 1483–1527, 2011

1 Introduction

Catastrophic boreal forest fires are expected to increase in the future, due to warmer and dryer conditions and longer fire seasons (Flannigan et al., 2009). The forest fires may affect air quality and feedback processes between climate and the biosphere, due to increases in atmospheric carbon dioxide (CO_2), pollutant gases, and aerosols (Bowman et al., 2009). Increases in the occurrence and extent of wildfires over the next 50–100 years may also transform the pathways and rates of transport of nutrients from the terrestrial ecosystems to marine ecosystems.

Iron-containing mineral aerosols may play a key role in ocean fertilization over significant portions of the surface ocean where macronutrients like nitrate are abundant but primary production and nitrogen fixation are limited by iron scarcity (Martin et al., 1994; Mills et al., 2004). The iron hypothesis (Martin, 1990) suggests that past increases in the supply of dust to the surface ocean during glacial stages decreased the effects of iron limitation on primary productivity. The resultant increase in the export of biogenic carbon from surface to deep ocean waters (i.e., the biological pump) could cause a decrease in atmospheric CO_2. The details of this process, and the possible magnitude of its effects on the global carbon cycle, are the subject of international debates (Maher et al., 2010; Bouttes et al., 2011).

Some Earth system models account for the effects of micronutrient limitations such as iron on oceanic photosynthesis. However, the model simulations can provide conflicting results regarding to the amount of atmospheric CO_2 captured by phytoplankton (Friedlingstein et al., 2006). One of the main reasons for these discrepancies is the estimation of how much iron is soluble in the ocean (Mahowald et al., 2009; Baker and Croot, 2010). Conventionally, dust is assumed as the major supplier of bioavailable iron with a constant solubility at 1–2% in the remote ocean, and intense forest fires are ignored.

BGD
8, 1483–1527, 2011

Field measurements suggest very intense fires could provide a source of atmospheric iron, which may be associated with dust particles entrained by pyro-convection (Gaudichet et al., 1995; Artaxo et al., 2002; Graham et al., 2003). Since iron from combustion sources is suggested to be more soluble than iron from dust (Chuang et al., 2005; Sedwick et al., 2007; Sholkovitz et al., 2009), biomass burning may have a pronounced effect on regional ocean fertilization (Guieu et al., 2005; Paris et al., 2010). The iron supplied from the biomass burning may influence climate feedback processes in terms of ocean CO_2 uptake and marine aerosol-cloud interactions, which may be induced by sulfate formation from dimethylsulfide (DMS) and carbon-containing aerosols produced from the ocean biomass (Charlson et al., 1987; O'Dowd et al., 2004; Boyd and Ellwood, 2010; Ito and Kawamiya, 2010).

Accurate estimates of biomass burning emissions are required for the assessment of aerosol deposition. The amount of biomass consumed during forest fires can vary significantly because of the spatial and temporal variation in the area burned as well as the quantity and quality of the fuels available for burning. Burned areas have been derived from remote sensing observations (Grégoire et al., 2003; Simon et al., 2004; Giglio et al., 2006) and have been widely used as an input for the estimation of the atmospheric emissions from biomass burning on a global scale (van der Werf et al., 2003; Hoelzemann et al., 2004; Ito and Penner, 2004). A growing number of satellite-based burned area products have been made available over the past several years (Langmann et al., 2009; Giglio et al., 2010). However, the MODerate resolution Imaging Spectroradiometer (MODIS) product underestimates the burned area in forests, due to insufficient cloud-free data during the fire season, and due to insufficient spatial resolution for quantifying fine-scale changes (Roy et al., 2008). In northern Eurasian forested regions, for example, the MODIS burned area product detected fewer fire-affected areas (10×10^3 km^2) than the active fire product (30×10^3 km^2). Underestimates in burned area from low resolution remotely sensed data might be calibrated by using high spatial resolution data (i.e., Landsat and ASTER) in forested regions (Eva and Lambin, 1998; Zhang et al., 2003; Huang et al., 2009). Potapov et al. (2008) used time-series data

BGD
8, 1483–1527, 2011

from MODIS and Landsat imagery to produce forest cover loss maps due to wildfires from 2001 and 2005. Their estimates showed significant increases in forest cover loss due to wildfires in Eurasia in 2002 and 2003, which are in line with other estimates of burned forest areas in Russia using the MODIS active fire detection product (Achard et al., 2008).

While interannual variations in emissions are largely driven by differences in area burned, the location of the fires relative to the availability of fuels and the timing of the fires during the burning season significantly influence emissions from boreal forest fires (Kasischke et al., 2005). In boreal Siberia, for instance, the carbon consumption estimates vary by more than an order of magnitude from 0.3 to 7.5 ($kg\,C\,m^{-2}$) (Soja et al., 2004). Thus fuel-load modeling at high spatial resolution would be required to improve estimates of emissions in combination with an accurate burned area data set (Ito and Penner, 2004; Hély et al., 2007; van der Werf et al., 2009). Moreover, emission estimates that consider variation in burned area but not variation in carbon consumption (2.2–8.3 $kg\,C\,m^{-2}$) could result in the underestimates of emissions in large-fire years (Turetsky et al., 2011). Fire season and area burned are the dominant factors that influence variability in the depth of soil organic matter consumed by forest fires (Soja et al., 2004; Kasischke et al., 2005; Turetsky et al., 2011). Thus fuel-consumption model needs to take into account both the fuel condition and fire severity to estimate variation in carbon consumption.

Accurate simulation of aerosol transport from forest fire emissions requires that the vertical distribution of smoke plumes is correctly described (Lavoué et al., 2000; Generoso et al., 2007; Hyer et al., 2007; Leung et al., 2007; Turquety et al., 2007). The vertical and horizontal extent of fire emissions by pyro-convection is a complex function of the heat flux, duration of burning, and local meteorology (Penner et al., 1986; Trentmann et al., 2006; Freitas et al., 2007; Val Martin et al., 2010). The use of injection height based on satellite observation may improve the model predictability of the transport pathways of forest fire emissions, when satellite observations are available (Chen et al., 2009; Gonzi and Palmer, 2010; Guan et al., 2010). Smoke plume injection

BGD
8, 1483–1527, 2011

height derived from the Multi-angle Imaging SpectroRadiometer (MISR) on board the Terra spacecraft is defined as the altitude at which the smoke particles are injected to the atmosphere before transport (Kahn et al., 2008).

Major forest fires have a large impact on atmospheric loadings of carbon monoxide (CO) and aerosols in the Northern Hemisphere (Cahoon et al., 1994; Tanimoto et al., 2000; Kajii et al., 2002; Kasischke and Bruhwiler, 2002). Enhanced CO columns and aerosol optical depths were observed over northeastern Russia in association with large forest fires in the summer of 2002 and over southeastern Russia in association with mega forest fires in the spring of 2003 (Edwards et al., 2004). The estimates of forest fire emissions might be evaluated by using an atmospheric chemistry transport model (CTM) and observation of CO near the source regions. The Measurements of Pollution in the Troposphere (MOPITT) product has been available for assessment of tropospheric CO (Deeter et al., 2003). The MOPITT product has been extensively validated using in situ CO measurements over a variety of geographical and seasonal cases including both monitoring and intensive field campaigns (Emmons et al., 2004, 2009; Deeter et al., 2010). As the most thoroughly validated satellite data set for CO, the MOPITT product has been widely used to constrain regional emissions (Arellano et al., 2004; Heald et al., 2004; Pétron et al., 2004).

The objective of this paper is to estimate the emissions from boreal forest fires based on a combined satellite data and modeling approach. These emission rates are used to examine the relative importance of biomass burning sources of soluble iron compared to those from dust sources. The focus of this paper is the deposition of soluble iron into the western North Pacific Ocean, which is a region that is particularly sensitive to iron fertilization (Tsuda et al., 2003; de Baar et al., 2005). In the following, Sect. 2 describes the biogeochemical and atmospheric chemical modeling approaches. Sect. 3 provides an evaluation of the simulated CO enhancements due to intense fires against satellite observations as well as implications of the mega fire emissions for future climate with regard to the ocean fertilization. Section 4 presents a summary of the findings and future remarks.

BGD
8, 1483–1527, 2011

2 Model approach

2.1 Biomass burning emission model

Satellite information of burned area, active fire, land cover and injection heights in conjunction with a biogeochemical model are used to estimate daily fire emissions in high latitude Northern Hemisphere regions (the extratropical, boreal and arctic areas north of 30° N latitude). The spatial (x, y, z) and temporal (t) variability in the atmospheric emissions ($[Q(i)]_{xyzt}$ g-species day^{-1}) for a specific species (i) from open vegetation fires can be described by the following equation:

$$[Q(i)]_{xyzt} = [\mathrm{BA}]_{xyt} \times [\mathrm{FL}]_{xyt} \times [\mathrm{CF}]_{xyt} \times [\mathrm{EF}(i)]_{xyt} \times [\mathrm{IH}]_{xyzt} \quad (1)$$

where BA is the burned area per day (m^2 day^{-1}), FL is the fuel load (kg-DM m^{-2}) expressed on a dry weight (DM) basis, CF is the combustion factor, EF is the emission factor (g-species kg-DM^{-1}), and IH is the vertical profile of fire injection height. The method follows a conventional bottom-up modeling approach (Seiler and Crutzen, 1980), with improvements summarized as follows:

1. Estimates of satellite-based area burned in forested regions were calibrated by using high spatial resolution data (Potapov et al., 2008, 2009).
2. Estimates of fuel load were calculated by using a biogeochemical model that was calibrated for an eastern Siberian forest (Sato et al., 2007, 2009).
3. The combustion factor for organic soil carbon was calculated as a function of the fire severity and fuel condition (Soja et al., 2004; Kasischke et al., 2005).
4. The injection height for the Siberian fires was derived from satellite observations (Kahn et al., 2008; Nelson et al., 2008).
5. Estimates of forest fire emissions are constrained by satellite measurement of CO (Deeter et al., 2010) in conjunction with CTM (Ito et al., 2007a, 2009).

BGD
8, 1483–1527, 2011

The focus of this paper is the boreal forest fire, which is separately described in Sect. 2.1.1. Emissions from temperate forests, grasslands/shrubs, wetlands, and croplands fires are also estimated in the high latitude Northern Hemisphere region (Sect. 2.2.2). The injection height of the fire emissions is described in Sect. 2.2.

2.1.1 Boreal forest

Annual areas affected by stand-replacement fires at a 20-km resolution in boreal forests are obtained from MODIS data calibrated by Landsat sample data (Potapov et al., 2008). In addition, the MODIS burned area data set (Roy et al., 2008) is used to identify the month of fires in boreal forests. In this study, the MODIS burned area data at the 500 m grid corresponding to non-vegetated areas (mainly classified as water bodies) are removed from the burned area maps, due to the application of a land cover map (Friedl et al., 2010). Day-to-day variations are obtained by using the Terra/MODIS version 5 level 3 daily thermal anomalies (i.e., hotspots or fires) product (Justice et al., 2002). The thermal anomalies that persist more than 12 days in a given year are classified as industrial thermal anomalies (Kovacs et al., 2004) and are not used in this study. The daily fire detection data at the 1000 m grid is used to identify the date of the fires. The analysis for the forest fires is separated into two fuel components, the aboveground component, which includes trees and herbaceous biomass above the ground surface, and the ground-layer organic material component, which includes partially decomposed organic matter in the upper portion of the soil. The aboveground (ground-layer) fires are assumed to last 1 day (8 days).

The fuel consumption model considers the herbaceous vegetation, the trees and the surface organic matter in forests. The carbon density is estimated from a global ecosystem model, the Spatially Explicit Individual-Based Dynamic Global Vegetation Model (SEIB-DGVM), which is described in detail in Sato et al. (2007). The model simulates the global terrestrial vegetation and soil dynamics in association with the carbon and water cycle. Establishment, mortality and competition among neighboring

BGD
8, 1483–1527, 2011

individual trees are taken into account by explicitly calculating tree height, crown diameter, crown depth, and light availability for each tree. The biogeochemical process-based model was calibrated for an eastern Siberian forest, based on field observations (Sato et al., 2009). The model includes a prognostic fire model, which could in principle simulate the pyrogenic emissions (Thonicke et al., 2001). For this study, the fire component embedded in the model is not used for the stand-replacement disturbance, but the simulated moisture content of the top soil layer is used as a fuel moisture index for determining the seasonal variation of the ground-layer fuel consumed. The climate data for the biogeochemical model were obtained from a previous simulation of the coupled climate-terrestrial carbon cycle model on a model grid of about 2.8° longitude by 2.8° latitude (T42) and averaged to daily values (Kato et al., 2009). The biases in the daily meteorological data were adjusted with monthly observation-based data from the Climatic Research Unit (CRU) (New et al., 2000). The biogeochemical model was run for 2000 years to bring the soil and vegetation carbon pools into equilibrium with climate.

The combustion factor (35%) for the aboveground biomass in boreal and temperate forests is taken from the literature (Kasischke et al., 2005), and is in line with the mean value (33%) measured in tropical forests (Ito and Penner, 2004). The combustion factor for the organic soil carbon is based on literature values (Soja et al., 2004; Kasischke et al., 2005), as a function of the fire severity and fuel condition, ranging from 8% to 100% (Table 1). Fire severity is widely used to describe the various impacts of a fire. In this paper, fire severity is directly related to the areas affected by fires per month and the type of fires (i.e., surface or stand-replacement) within a 0.5° grid cell. During the late burning season from August to October, it is assumed that the surface organic layer is under a dry condition, resulting in deeper burning (Kasischke et al., 2005). Then, the combustion factor for stand-replacement fires is scaled exponentially to the minimum value (23%) from the maximum value (100%) under high severity conditions, based on the soil moisture index. Additionally, all fire events that consume more than 100 km^2 $month^{-1}$ are assumed to be a large and severe fire (Soja et al., 2004). Then,

BGD
8, 1483–1527, 2011

the combustion factor in areas less than high severity (> 100 km^2 $month^{-1}$) is scaled linearly based on the area burned to the minimum values under low severity conditions.

In estimating the contribution of each gas species and aerosol to the emissions, the proportion of flaming and smoldering burning is considered for each fuel component to account for differences in emission factors for these two combustion types. The emission factors of CO, nitrogen oxide (NO) and particulate matter less than 2.5 µm in diameter ($PM_{2.5}$) for aboveground (116 g-CO kg-DM^{-1}, 2.3 g-NO kg-DM^{-1} and 12 g-$PM_{2.5}$ kg-DM^{-1}) and ground-layer (193 g-CO kg-DM^{-1}, 1.0 g-NO kg-DM^{-1} and 18 g-$PM_{2.5}$ kg-DM^{-1}) fires in forests are obtained from literature data (Kasischke and Bruhwiler, 2002; Reid et al., 2005; Lapina et al., 2008). The emission factors for non-methane volatile organic compounds (NMVOCs) and coarse particles are calculated using the emission factors in extratropical forests (Andreae and Merlet, 2001). The averaged iron fraction measured over downwind regions of biomass burning is used for coarse particles (3.4%) (Fuzzi et al., 2007), which is consistent with that in mineral dust of 3.5% (Duce and Tindale, 1991). For biomass burning aerosols, fine particulate matter is primarily carbonaceous, while the dryer climate and the enhanced convection during intense forest fires are expected to increase dust related elements in the atmosphere (Gaudichet et al., 1995; Artaxo et al., 2002; Graham et al., 2003). Thus the iron fractions in the fine particles are related to the combustion stages of flaming (0.46 ± 0.51%), which is consistent with the value for aged regional smoke (0.47 ± 0.21%), and smoldering (0.06 ± 0.03%) fires (Reid et al., 2005).

2.1.2 Temperate forest, grassland, wetland and cropland

Emissions from temperate forests, grasslands/shrubs, wetlands, and croplands fires are estimated primarily based on the methods described in Sect. 2.1.1. The major difference is that the MODIS data of stand-replacement burned area calibrated by the Landsat sample data were not available as a separate class in temperate forests. Thus the combination of burned area data (Roy et al., 2008) and tree cover data calibrated

BGD
8, 1483–1527, 2011

by the Landsat sample data (Hansen et al., 2003, 2010; Potapov et al., 2009) is used to estimate the amount of stand-replacement burned area in temperate forests. It is assumed that the fractional tree cover that burns in a given time period may be approximated from the difference between tree cover data obtained from different years. Thus the change in the tree cover percentage as determined from the satellite image interpretation is used to differentiate whether or not crown fires occur. The analysis of forest cover loss due to fires is performed only for areas covered by forest, which is defined as 500 m MODIS pixels with tree canopy cover greater than 25% based on the tree cover data set for the year of 2000. For crown fires occurring in temperate forests, the previous and current annual tree cover areas are regarded as the pre- and post-fire tree cover areas, respectively, when the area is associated with a non-zero MODIS fire-affected area. The visual inspection of Landsat sample blocks reveals that the majority of forest cover loss in temperate forests is due to mechanical forest cover removal (78%) and, to a lesser extent fires (11%) and the combination of mechanical clearing and fire (11%) (Potapov et al., 2009). Moreover, the forest cover loss is mostly observed within southern temperate forests in China. Therefore, the potential underestimate in temperate forest fires is not expected to have a large influence on the conclusions in this paper. The rest of the differences in the methods are briefly described below.

While the forest fires are classified as crown and surface fires, other types of fires consume part of the carbon at the ground surface. The MODIS products of fire count (Justice et al., 2002), burned area (Roy et al., 2008), and land cover (Hansen et al., 2003, 2010; Potapov et al., 2009; Friedl et al., 2010) are used to estimate daily surface area burned in boreal and temperate regions. Amounts of monthly burned areas associated with each land cover (except where the fire-affected area overlaps with the forest cover loss) are calculated using the burned area and land cover. It is assumed that the entire 500 m × 500 m grid cell in which MODIS detects a fire-affected area is subject to burning even though the fires that are detected might be smaller than this grid cell. Then, the monthly burned area data are distributed to daily data using the fire

BGD
8, 1483–1527, 2011

counts. The fuel consumption model for the surface fires considers herbaceous vegetation in grasslands/shrubs, croplands, wetlands and forests. In addition, the surface organic matter is taken into account as fuel in wetlands and forests. To account for the spatial and seasonal variation in CF and EF (Ito et al., 2007b and references therein), the CF and EF for the aboveground fuels are determined from the satellite observation of Normalized Difference Vegetation Index (NDVI) (Huete et al., 2002) except those for forests and soil organic carbon, which are described in Sect. 2.1.1.

2.2 Atmospheric chemistry and aerosol transport model

The Integrated Massively Parallel Atmospheric Chemical Transport (IMPACT) model was developed at the Lawrence Livermore National Laboratory (LLNL) (Rotman et al., 2004) but was extended to treat aerosols (Liu et al., 2005; Feng and Penner, 2007) and detailed chemical reactions for a wider set of volatile organic compounds (Ito et al., 2007a) at the University of Michigan. The detailed gas-phase chemistry version of the IMPACT model (Ito et al., 2007a, 2009) is used to calculate atmospheric CO mixing ratio. The model is driven by assimilated meteorological fields from the Goddard Earth Observation System (GEOS) of the NASA Global Modeling and Assimilation Office (GMAO). Simulations were performed at three different horizontal resolutions: low resolution ($4^\circ \times 5^\circ$), middle ($2^\circ \times 2.5^\circ$) and high ($1^\circ \times 1^\circ$). The emissions of precursor gases, chemistry of gas-phase and heterogeneous reactions, dry and wet deposition, are simulated.

The global biomass burning emissions data set during 2001–2005 (except the high latitude Northern Hemisphere) is as described in Ito et al. (2009), which is based on the emissions data developed by Ito and Penner (2004) and Ito et al. (2007b). The anthropogenic fossil fuel and biofuel emissions data are taken from the RETRO emission data set for 2000 (Schultz and Rast, 2007). It is acknowledged that the burning of biofuel for industrial or residential purposes and the burning of agricultural residues are treated as part of the anthropogenic activities in the RETRO emission inventories. Thus the biomass burning emission rates except for croplands that are estimated in

BGD
8, 1483–1527, 2011

this paper are added to these input data for the gas-phase chemistry transport model. The chemical production of CO from the oxidation of hydrocarbons and the loss of CO via the reaction of CO with OH are calculated from the online simulations of gas-phase chemistry.

Four separate simulations of the CTM are performed: (Exp 1) uses monthly emissions at the coarsest CTM grid ($4^\circ \times 5^\circ$), (Exp 2) uses daily emissions at the coarsest CTM grid, (Exp 3) uses daily emissions at the middle CTM grid ($2^\circ \times 2.5^\circ$), and (Exp 4) uses daily emissions at the finest CTM grid ($1^\circ \times 1^\circ$). The standard simulation was conducted (Exp 1) with monthly emissions from 2001 to 2005 after a 6-month spin-up time. For the standard simulation, biomass burning emissions are assumed to take place in the lowest model-layer. Sensitivity simulations (Exp 2–4) with daily emissions at the three different resolutions were performed for two large fires in August 2002 and May 2003, with initial conditions taken from the standard simulation and a 3-month spin-up time. In the sensitivity simulations, the median height for each plume derived from MISR is used to determine the daily injection height for large fires (Kahn et al., 2007, 2008; Nelson et al., 2008). In this approach, when the height of a smoke plume or cloud is more than 2 km above terrain, as observed by MISR, the emissions in the model grid box containing the plume are released to the model layer corresponding to the MISR-derived plume height (Chen et al., 2009). When a number of smoke plumes were observed at different altitudes within the same model grid and for the same date, the relative amounts of emissions were calculated by weighting the contribution from each plume by its digitized area (Nelson et al., 2008). The rest plumes of the boreal forest fire emissions are assumed to be emitted near the surface and quickly mixed throughout the planetary boundary layer (PBL). Therefore, other boreal forest fire emissions are evenly distributed in mixing ratio throughout the PBL.

Satellite observations of CO from the Terra/MOPITT version 4 level 3 product (Deeter et al., 2010) are used to evaluate the model performance in simulating the spatial and temporal patterns of the fire emissions. The MOPITT version 4 product embodies algorithm enhancements which improve retrieval performance in very clean and also

BGD
8, 1483–1527, 2011

polluted conditions. To make a proper comparison between the MOPITT retrievals with the model output, the modeled CO profile collected during daytime MOPITT overpasses was transformed using the MOPITT a priori profile and the averaging kernels. For comparison of pollutant burdens, the total column mass for CO in units of (molecules cm^{-2}) was calculated from the CO profile using the hydrostatic relation, as described by Emmons et al. (2004).

For the simulation of aerosols, the aerosol chemistry version of the IMPACT model is used (Liu et al., 2005; Feng and Penner, 2007; Ito and Feng, 2010). Emissions of primary particles and precursor gases, chemistry of gas-phase, heterogeneous, and aqueous-phase reactions including a mineral dissolution scheme, and dry and wet deposition are simulated. A daily dust emission data set is used for the simulation of mineral aerosols (Dentener et al., 2006). The emissions for Asian dust in April were scaled to obtain a better agreement with aircraft observations by Ito and Feng (2010). Thus the global and Asian dust emissions for April–May are 289 and 49 Tg, which are comparable to those (321 and 33 Tg) simulated by Fairlie et al. (2007). The monthly emission data set (except the open biomass burning emissions data in the high latitude Northern Hemisphere) is used for the simulation of combustion-generated aerosols as described in Ito and Feng (2010). The initial conditions for soluble iron fractions from the dust (0.45%) and combustion sources (4%) are prescribed (Luo et al., 2008). The iron dissolution in dust aerosols due to atmospheric chemical processing is calculated from the online simulation of aerosol-phase chemistry, which quantitatively reproduces higher iron solubility in smaller particles (Ito and Feng, 2010), as suggested by the onboard cruise measurements over the Pacific Ocean (Chen and Siefert, 2003). To examine the potential impact of extreme fire events on soluble iron deposition, the biomass burning emission rates estimated in this paper are used as revised input data for the aerosol chemistry transport model. The transport and deposition of the fine (coarse) iron particles from biomass burning sources are treated similarly to black carbon (coarse-mode dust aerosol). The combustion-generated iron particles are externally mixed with other aerosols in the model, assuming that the combustion-generated

BGD
8, 1483–1527, 2011

iron on the particle surface has a labile chemical form without atmospheric processing by anthropogenic pollutants (Schroth et al., 2009). Simulations of the CTM are performed (Exp 5) with the daily emissions from boreal forest fires using the $2^\circ \times 2.5^\circ$ horizontal resolution. As described for the gas-phase chemistry model, the boreal forest fire emissions depend on the MISR-derived injection height. The model was spun up for two months before the production runs.

3 Results and discussion

3.1 Biomass burning emission

The burned areas estimates show large interannual variations in the areas burned in forested regions during 2001–2005 ($13–51 \times 10^3\ km^2\ yr^{-1}$), compared to the total areas burned ($256–480 \times 10^3\ km^2\ yr^{-1}$) in the high latitude Northern Hemisphere (Table 2). Fuel consumption in the model depends on the fuel load and combustion factor. The spatial distribution of carbon consumption estimates ($kg\,C\,m^{-2}$ of area burned) generally resembles the fuel load distribution, since land cover types with high biomass density (i.e., forests) store more fuels available to burn than those with low biomass density (i.e., grasslands) (Fig. 1a). Additionally, the combustion factor for soil organic carbon is increased in forested areas when high-severity crown fires occur in dry conditions. As a consequence, significant interannual variation of carbon consumption is found over boreal forests, especially east of Lake Baikal (Fig. 1b). Accordingly, the spatial and temporal differences in carbon consumption estimates demonstrate the importance of describing the quantity and quality of fuels consumed in varying regions and times for estimates of total direct carbon emitted.

The carbon consumption estimates in eastern Siberian forests ($5–10\,kg\,C\,m^{-2}$) are about double those ($2–5\,kg\,C\,m^{-2}$) for the average over 1997–2009 as calculated by van der Werf et al. (2010) but more similar to the observation-based estimates for high-severity fires by Soja et al. (2004) and Turetsky et al. (2010). This is primarily because

BGD
8, 1483–1527, 2011

the burned area data only quantifies those areas affected by stand-replacement fires (Potapov et al., 2008). The intent of this study is the estimation of emissions from extremely large fires, which are hypothesized to influence the ocean fertilization.

There is a significant spatial and interannual variability of annual CO emissions (12–78 Tg CO yr^{-1}) in the high latitude Northern Hemisphere (Fig. 2). The largest contribution to emissions in 2002 and 2003 is from forest fires in eastern Siberia. In contrast, the largest contribution to emissions in 2004 is from large fires, which include a large contribution from peat burning, in Alaska and western Canada (Pfister et al., 2005; Turquety et al., 2007). These differences emphasize the importance of determining the amount of fuel consumed in the partially decomposed soil organic matter.

The annual CO emission from Russian fires (40–90° N; 60–180° E) in 2003 (60 Tg) is in the low range of the estimates reported in the literature (53–160 Tg) (Jaffe et al., 2004; Kasischke et al., 2005; Yurganov et al., 2005; Generoso et al., 2007). Generoso et al. (2007) increased their estimate at the lower end of the range in their model in order to obtain a better agreement with the observations, which were influenced by the outflow from the boreal fires. The estimate of CO emissions in May 2003 (22 Tg) is in the middle of their scaled estimates (15–30 Tg).

3.2 Spatial distribution and temporal variation of CO

In this section, simulated and observed CO columns are compared over the primary region disturbed by the forest fires in eastern Siberia. To obtain sufficient MOPITT data for comparison purposes, the hourly data of model results and MOPITT observations were collected for each month from 2001 to 2005 and over the domain, ranging from 40° to 70° N in latitude and from 100° to 140° E in longitude. Then, the averages and standard deviations are calculated from the hourly values. The model simulates the general seasonal and interannual patterns of CO columns over eastern Siberia (Fig. 3). The monthly averaged CO columns are generally low in summer due to enhanced destruction of CO by the OH radical, except for the large fire seasons in 2002 and 2003. The model result of CO ($1.8 \pm 0.3 \times 10^{18}$ molecules cm^{-2}) is consistently lower than the

BGD
8, 1483–1527, 2011

MOPITT data ($2.1 \pm 0.2 \times 10^{18}$ molecules cm^{-2}), which mainly reflects an underestimate of the background CO mixing ratio in the model. Models (including the CTM used in this study) typically show systematic underestimates of Northern Hemisphere extratropical CO throughout the year, probably due to the underestimation of surface CO emissions from anthropogenic sources (Shindell et al., 2006). A more recent modeling study uses an updated emission inventory, but still indicates the underestimates of CO (Lamarque et al., 2010). Further investigation is required to fully understand the reason for the low bias in background CO.

The model results of monthly averaged CO ($\times 10^{18}$ molecules cm^{-2}) are in reasonably good agreement with MOPITT observations during the large (1.8–2.0 vs. 2.3 ± 0.2) and mega (2.2–2.3 vs. 2.8 ± 0.4) fire months (Table 3). Enhancements due to the different intensities of fire emissions are calculated from the differences in CO between the two different months for large and mega fires. The modeled enhancement of CO due to the intensified fires is consistent with that from observations (0.3–0.4 vs. 0.4 ± 0.1). This result suggests that the model using emissions estimated in this work is able to describe the interannual changes in CO due to different strengths of forest fires.

The simulated CO columns are compared between different numerical experiments (Exp 1–4) to assess the uncertainties in the model response over eastern Siberia (Table 3). The large differences between the finest resolution values (Exp 4) and the other experimental values (Exp 1–3) are only found in the immediate vicinity of strong sources. The differences in CO columns at the grid cell level include both negative and positive values which are mostly averaged out when comparing the regional values. As a result, the differences in the averages between the Exp 4 and the others (Exp 1–3) ($< 10\%$ in Table 3) are less than those between the model results (Exp 1–4) and observations (13–22%). Since the Exp 3 uses the same spatial resolution of the CTM as the aerosol simulation (Exp 5), hereafter we use only the results from Exp 3 for comparison with observations unless otherwise specified.

The model simulates the general spatial pattern of observed CO columns (Fig. 4), although as noted above the modeled CO ($\times 10^{18}$ molecules cm^{-2}) tends to be lower than

BGD
8, 1483–1527, 2011

the MOPITT data (the monthly averaged differences are −0.2 ($\times 10^{18}$ molecules cm^{-2}) in August 2002 and −0.4 in May 2003). Both the model result and MOPITT observation capture the high CO burdens ($\times 10^{18}$ molecules cm^{-2}) from Siberian forest fires over northeastern Russia in August 2002 (2.5–3.5) and over southeastern Russia in May 2003 (3–5). However, there are some spatial differences in the CO column between model and observation near the strong source regions in May 2003, which are discussed later.

The shape of simulated CO vertical profile is consistent with that of the MOPITT data, although the value of the simulated CO mixing ratio is consistently lower than the MOPITT data (Fig. 5). In August 2002, more elevated CO columns are seen over northeastern Russia (60°–70° N; 120°–140° E), while in May 2003, much more elevated CO clumns are found over southeastern Russia (40°–60° N; 110°–140° E) than in other eastern Siberian regions. The elevated levels of CO mixing ratio can be attributed to the influence from intense fires. Thus the enhancements in the CO mixing ratio due to strong fires can be calculated from the differences between the data averaged over the strong source areas and over the eastern Siberian regions excluding the strong source areas. As a result, the regionally averaged enhancement of observed CO mixing ratio due to forest fires is well captured by the model. The enhancements of CO at the surface (model vs. observation) due to strong fires in May 2003 (67% vs. 66%) are significantly higher than those in August 2002 (22% vs. 19%). These results suggest that the regionally averaged amount of fire emissions and vertical profile of CO mixing ratio are well reproduced by the model. However, the model CO mixing ratio is lower than observation at higher altitudes (by 25% at 700 hPa) in May 2003, although the difference is within the observational standard deviation for the monthly and regionally average.

To investigate the underestimates in CO near the strong source locations at higher altitudes in May 2003, the spatial distribution of CO mixing ratio is compared between five different levels, ranging from the surface pressure to 600 hPa (Fig. 6). The high mixing ratio of CO (i.e., hot spot) in the surface air due to Siberian forest fires is well

BGD
8, 1483–1527, 2011

reproduced by the model. However, the MOPITT observations show that hot spot locations (> 400 ppb) at higher altitude (700 hPa) are further from Lake Baikal than those at lower altitude (900 hPa). These results may reflect that the timing of intense fires is not correctly captured by the model. It should be noted that MOPITT detects the different hot spot locations at 900 hPa and at 700 hPa on different days, since MOPITT only provides a near-global distribution of CO every 3 days. The modeled day-to-day variation of intense fire emissions strongly depends on the MODIS fire count. The hot spot locations at higher altitudes, as suggested by the measurements, are not seen after extracting the simulated data from the raw model output for comparison with the MOPITT data and monthly averaging the daily data. However, the pronounced increases in the CO mixing ratio at higher altitudes are seen from the raw data in the same areas but for different days when there are no MOPITT data. Thus errors due to the allocations of intense fire emissions to different times under different meteorological conditions significantly contribute to the variation error in the spatial distribution of CO on a daily basis in the vicinity of the strong source locations. The differences in monthly CO averages between the model results and observations become smaller as the air masse ages.

3.3 Potential impact of intense fires on ocean fertilization

In this section, the potential effect of the Siberian fires in terms of atmospheric soluble iron supply to the ocean is investigated by comparison with that of Asian dust. One might expect to validate the model results with the aerosol optical depths. However, there are many more factors that affect aerosol optical depths than simply the emissions (Textor, et al., 2007). Therefore the model results are not discussed in the context of the aerosol optical properties in this paper, but this is an important issue that deserves future work.

Asian dust-storm particles originating from the deserts and loess areas are often transported over Japan and the Pacific Ocean in the boreal spring (Iwasaka et al., 1983; Uematsu et al., 1983). Thus the simulated soluble iron deposition from dust sources in

BGD
8, 1483–1527, 2011

May is larger than that in August (Fig. 7). Compared with the dust sources, combustion sources (with the MISR-derived injection heights of daily boreal forest fire emissions) significantly contribute to deposition of soluble iron (10–40%) into the western North Pacific Ocean in May. The soluble iron deposition from combustion sources in August is more localized over the source regions than that in May. These results reflect the influence of the higher injection height for the simulation with intense emissions, since the particles injected in the free troposphere are transported over longer distances, because of the increased wind and reduced deposition. When the aerosols are injected above the PBL, wet deposition is dominant removal process for the fine mode particles. On the other hand, when the aerosols are emitted in the surface layer, the particles are efficiently scavenged via dry deposition near the source regions.

The injection of nutrients above the PBL due to forest fires has important implications for the future climate (Flannigan et al., 2009) as well as for climate in the preindustrial period (Marlon et al., 2008; Wang et al., 2010) when emissions from biomass burning are considered to be significant. Also, global warming has been predicted to intensify the stratification of the upper ocean, reduce vertical mixing, and supply fewer nutrients from the deep ocean to the surface ocean. This situation may make oceanic primary production more dependent on the nutrient input from atmospheric aerosols. Furthermore, sulfur dioxide emissions are projected to decrease over the next century according to the Representative Concentration Pathways (RCPs) scenarios (Van Vuuren et al., 2010). Accordingly, iron dissolution due to the acid mobilization of the iron-containing minerals could be reduced. Compared to the delivery of soluble iron from dust sources without the atmospheric processing by acidic species, combustion sources dominantly contribute to deposition of soluble iron (10–60%) into the western North Pacific Ocean during extreme fire events (Fig. 8). It may imply that the supply of nutrients from large forest fires plays a role as a negative biosphere-climate feedback, due to increases in the amount of ocean uptake of CO_2 and emissions of marine biogenic aerosols and trace gases.

BGD
8, 1483–1527, 2011

4 Conclusions

Aerosols and trace gases emitted from large forest fires in eastern Siberia may affect air quality and climate. Assessment of these effects needs an accurate characterization of the spatial distribution and temporal variability of intense fire emissions. Improvements in estimates of satellite-based burned area, fuel consumption using a biogeochemical model, and injection heights derived from satellite observations in eastern Siberia were examined together with improved accuracy of satellite measurements of carbon monoxide in conjunction with an atmospheric chemistry transport model. Comparison of modeled CO to satellite observations suggests that the methodology successfully captured the atmospheric CO enhancements due to intense forest fires. The use of daily biomass burning emissions together with the injection of fire emissions above the PBL slightly improved agreement with MOPITT CO measurements (Table 3).

The emission rates from the intense fires are applied to the aerosol chemistry transport model to examine the relative importance of biomass burning sources of soluble iron compared to those from dust sources. For the first time, the simulation results suggest that extreme fire events may be dominant sources of soluble iron over the western North Pacific Ocean, especially when the emissions of acid gases are suppressed. Given the large uncertainties in the quantification of dissolved iron in the sea water, the forest fire as a potential supply of soluble iron should not be ignored. Also, given the significant emissions from biomass burning in a warmer period, the fires may be important to simulate the effect of iron on ocean fertilization and need to be introduced as a potential feedback in the models. While an attempt can be made to couple the negative biosphere-climate feedback in Earth system models, fundamental work is needed on iron speciation in mineral aerosols, transformation to soluble iron in the atmosphere, and availability to ocean biota (Carslaw et al., 2010). The information on the spatial and temporal distributions of emissions associated with local meteorological conditions is critical in improving the deposition rates of aerosols to the ocean. Further works is required to improve quantitative, episodic, and predictive capabilities of the aerosol simulation from forest fires. In particular, a model approach for predicting the

BGD
8, 1483–1527, 2011

vertical transport of smoke particles will be needed to integrate the fire module into Earth system model for projecting an Earth system dynamics. It should be noted that the iron fraction in biomass burning aerosols is highly uncertain, ranging from 0.02% to 1.2% for fine particles during flaming combustion (Reid et al., 2005). Clearly, field measurements of the iron fraction in the fine particles are needed to improve the estimate of iron deposition from the intense forest fires to the ocean. Moreover, the iron solubility observed for biomass burning aerosols varies by more than an order of magnitude from 0.5% to 6.5% (Guieu et al., 2005; Paris et al., 2010). Further research involving laboratory experiments, modeling, and observations is desirable for understanding the process that increases iron solubility from minerals in biomass burning air masses.

Acknowledgements. Support for this research was provided to A. Ito by Innovative Program of Climate Change Projection for the 21st Century (MEXT). All of the numerical simulations in this study were performed using the SGI Altix4700 at the JAMSTEC. The MODIS burned area, active fire, land cover, and NDVI products are distributed by the Land Processes Distributed Active Archive Center (LP DAAC), located at the U.S. Geological Survey (USGS) Earth Resources Observation and Science (EROS) Center (lpdaac.usgs.gov). The MOPITT and MISR data were obtained from the NASA Langley Research Center Atmospheric Science Data Center. The author is grateful to J. E. Penner at the University of Michigan for constructive comments that helped to improve this paper significantly.

References

Achard, F., Eva, H. D., Mollicone, D., and Beuchle, R.: The effect of climate anomalies and human ignition factor on wildfires in Russian boreal forests, Phil. Trans. R. Soc. B, 363, 2331–2339, doi:10.1098/rstb.2007.2203, 2008.

Andreae, M. O. and Merlet, P.: Emission of trace gases and aerosols from biomass burning, Glob. Biogeochem. Cy., 15, 955–966, 2001.

Arellano Jr., A. F., Kasibhatla, P. S, Giglio, L., van der Werf, G. R., and Randerson, J. T.: Top-down estimates of global CO sources using MOPITT measurements, Geophys. Res. Lett., 31, L01104, doi:10.1029/2003GL018609, 2004.

Artaxo, P., Martins, J. V., Yamasoe, M. A., Procpio, A. S., Pauliquevis, T. M., Andreae, M. O., Guyon, P., Gatti, L. V., and Leal, A. M. C.: Physical and chemical properties of aerosols in the wet and dry seasons in Rondônia, Amazonia, J. Geophys. Res., 107, 8081, doi:10.1029/2001JD000666, 2002.

Baker, A. R. and Croot, P. L.: Atmospheric and marine controls on aerosol iron solubility in seawater, Mar. Chem., 120, 4–13, doi:10.1016/j.marchem.2008.09.003, 2010.

Bouttes, N., Paillard, D., Roche, D. M., Brovkin, V., and Bopp, L.: Last Glacial Maximum CO_2 and $\delta^{13}C$ successfully reconciled, Geophys. Res. Lett., 38, L02705, doi:10.1029/2010GL044499, 2011.

Bowman, D. M. J. S., Balch, J. K., Artaxo, P., Bond, W. J., Carlson, J. M., Cochrane, M. A., D'Antonio, C. M., DeFries, R. S., Doyle, J. C., Harrison, S. P., Johnston, F. H., Keeley, J. E., Krawchuk, M. A., Kull, C. A., Marston, J. B., Moritz, M. A., Prentice, I. C., Roos, C. I., Scott, A. C., Swetnam, T. W., van der Werf, G. R., and Pyne, S. J.: Fire in the Earth System, Science, 324, 481–484, doi:10.1126/science.1163886, 2009.

Boyd, P. W. and Ellwood, M. J.: The biogeochemical cycle of iron in the ocean, Nat. Geosci., 3, 675–682, doi:10.1038/ngeo964, 2010.

Cahoon Jr., D. R., Stocks, B. J., Levine, J. S., Cofer III, W. R., and Pierson, J. M.: Satellite analysis of the severe 1987 forest fires in northern China and southeastern Siberia, J. Geophys. Res., 99, 18627–18638, 1994.

Carslaw, K. S., Boucher, O., Spracklen, D. V., Mann, G. W., Rae, J. G. L., Woodward, S., and Kulmala, M.: A review of natural aerosol interactions and feedbacks within the Earth system, Atmos. Chem. Phys., 10, 1701–1737, doi:10.5194/acp-10-1701-2010, 2010.

Charlson, R. J., Lovelock, J. E., Andreae, M. O., and Warren, S. G.: Oceanic phytoplankton, atmospheric sulfur, cloud albedo and climate, Nature, 326, 655–661, doi:10.1038/326655a0, 1987.

Chen, Y. and Siefert, R.: Determination of various types of labile atmospheric iron over remote oceans, J. Geophys. Res., 108, 4774, doi:10.1029/2003JD003515, 2003.

Chen, Y., Li, Q., Randerson, J. T., Lyons, E. A., Kahn, R. A., Nelson, D. L., and Diner, D. J.: The sensitivity of CO and aerosol transport to the temporal and vertical distribution of North American boreal fire emissions, Atmos. Chem. Phys., 9, 6559–6580, doi:10.5194/acp-9-6559-2009, 2009.

Chuang, P. Y., Duvall, R. M., Shafer, M. M., and Schauer, J. J.: The origin of water soluble particulate iron in the Asian atmospheric outflow, Geophys. Res. Lett., 32, L07813,

doi:10.1029/2004GL021946, 2005.
de Baar, H. J. W., Boyd, P. W., Coale, K. H. , Landry, M. R., Tsuda, A., Assmy, P., Bakker, D. C. E., Bozec, Y., Barber, R. T., Brzezinski, M. A., Buesseler, K. O., Boye, M., Croot, P. L., Gervais, F., Gorbunov, M. Y., Harrison, P. J., Hiscock, W. T., Laan, P., Lancelot, C., Law, C. S., Levasseur, M., Marchetti, A., Millero, F. J., Nishioka, J., Nojiri, Y., van Oijen, T., Riebesell, U., Rijkenberg, M. J. A., Saito, H., Takeda, S., Timmermans, K. R., Veldhuis, M. J. W., Waite, A. M., and Wong, C. S.: Synthesis of iron fertilization experiments: From the iron age in the age of enlightenment, J. Geophys. Res., 110, C09S16, doi:10.1029/2004JC002601, 2005.
Deeter, M. N., Emmons, L. K., Francis, G. L., Edwards, D. P., Gille, J. C., Warner, J. X., Khattatov, B., Ziskin, D., Lamarque, J.-F., Ho, S.-P., Yudin, V., Attie, J.-L., Packman, D., Chen, J., Mao, D., and Drummond, J. R.: Operational carbon monoxide retrieval algorithm and selected results from the MOPITT instrument, J. Geophys. Res., 108, 4399, doi:10.029/2002JD003186, 2003.
Deeter, M. N., Edwards, D. P., Gille, J. C., Emmons, L. K., Francis, G., Ho, S.-P., Mao, D., Masters, D., Worden, H., Drummond, J. R., and Novelli, P. C.: The MOPITT version 4 CO product: Algorithm enhancements, validation, and long-term stability, J. Geophys. Res., 115, D07306, doi:10.1029/2009JD013005, 2010.
Dentener, F., Kinne, S., Bond, T., Boucher, O., Cofala, J., Generoso, S., Ginoux, P., Gong, S., Hoelzemann, J. J., Ito, A., Marelli, L., Penner, J. E., Putaud, J.-P., Textor, C., Schulz, M., van der Werf, G. R., and Wilson, J.: Emissions of primary aerosol and precursor gases in the years 2000 and 1750 prescribed data-sets for AeroCom, Atmos. Chem. Phys., 6, 4321–4344, doi:10.5194/acp-6-4321-2006, 2006.
Duce, R. A. and Tindale, N. W.: Atmospheric transport of iron and its deposition in the ocean, Limnol. Oceanogr., 36(8), 1715–1726, 1991.
Edwards, D. P., Emmons, L. K., and Hauglustaine, D. A., Chu, A., Gille, J. C., Kaufman, Y. J., Petron, G., Yurganov, L. N., Giglio, L., Deeter, M. N., Yudin, V., Ziskin, D. C.,Warner, J., Lamarque, J. -F., Francis, G. L., Ho, S. P., Mao, D., Chen, J., Grechko, E. I., and Drummond, J. R.: Observations of carbon monoxide and aerosols from the Terra satellite: Northern Hemisphere variability, J. Geophys. Res., 109, D24202, doi:10.1029/2004JD004727, 2004.
Emmons, L. K., Deeter, M. N., Gille, J. C., Edwards, D. P., Attie, J.-L., Warner, J. Ziskin, D., X., Francis, G. L., Khattatov, B., Yudin, V., Lamarque, J.-F., Ho, S.-P., Mao, D., Chen, J., Drummond, J. R., Novelli, P. C., Sachse, G., Coffey, M. T., Hannigan, J. W., Gerbig, C., Kawakami, S., Kondo, Y., Takegawa, N., Schlager, H., Baehr, J., and Ziereis, H.: Validation

BGD
8, 1483–1527, 2011

of Measurements of Pollution in the Troposphere (MOPITT) CO retrievals with aircraft in situ profiles, J. Geophys. Res., 109, D03309, doi:10.1029/2003JD004101, 2004.
Emmons, L. K., Edwards, D. P., Deeter, M. N., Gille, J. C., Campos, T., Nédélec, P., Novelli, P., and Sachse, G.: Measurements of Pollution In The Troposphere (MOPITT) validation through 2006, Atmos. Chem. Phys., 9, 1795–1803, doi:10.5194/acp-9-1795-2009, 2009.
Eva, H. and Lambin, E. F.: Remote sensing of biomass burning in tropical regions: sampling issues and multisensor approach, Rem. Sens. Environ., 64, 292–315, 1998.
Fairlie, T. D., Jacob, D. J., and Park, R. J.: The impact of transpacific transport of mineral dust in the United States, Atmos. Environ., 41, 1251–1266, 2007.
Feng, Y. and Penner, J. E.: Global modeling of nitrate and ammonium: Interaction of aerosols and tropospheric chemistry, J. Geophys. Res., 112, D01304, doi:10.1029/2005JD006404, 2007.
Flannigan, M., Stocks, B., Turetsky, M., and Wotton, M.: Impacts of climate change on fire activity and fire management in the circumboreal forest, Global Change Biol., 15, 549–560, doi:10.1111/j.1365-2486.2008.01660.x, 2009.
Freitas, S. R., Longo, K. M., Chatfield, R., Latham, D., Silva Dias, M. A. F., Andreae, M. O., Prins, E., Santos, J. C., Gielow, R., and Carvalho Jr., J. A.: Including the sub-grid scale plume rise of vegetation fires in low resolution atmospheric transport models, Atmos. Chem. Phys., 7, 3385–3398, doi:10.5194/acp-7-3385-2007, 2007.
French, N. H. F., Goovaerts, P., and Kasischke, E. S.: Uncertainty in estimating carbon emissions from boreal forest fires, J. Geophys. Res., 109, D14S08, doi:10.1029/2003JD003635, 2004.
Friedl, M. A., Sulla-Menashe, D., Tan, B., Schneider, A., Ramankutty, N., Sibley, A., and Huang, X.: MODIS collection 5 global land cover: Algorithm refinements and characterization of new datasets, Rem. Sens. Environ., 114, 168–182, 2010.
Friedlingstein, P., Cox, P., Betts, R., Bopp, L., von Bloh, W., Brovkin, V., Cadule, P., Doney, S., Eby, M., Fung, I., Bala, G., John, J., Jones, C., Joos, F., Kato, T., Kawamiya, M., Knorr, W., Lindsay, K., Matthews, H. D., Raddatz, T., Rayner, P., Reick, C., Roeckner, E., Schnitzler, K.-G., Schnur, R., Strassmann, K., Weaver, A. J., Yoshikawa, C., and Zeng, N.: Climate-carbon cycle feedback analysis: Results from the C4MIP model intercomparison, J. Clim., 19, 3337–3353, 2006.
Fuzzi, S., Decesari, S., Facchini, M. C., Cavalli, F., Emblico, L., Mircea, M., Andreae, M. O., Trebs, I., Hoffer, A., Guyon, P., Artaxo, P., Rizzo, L. V., Lara, L. L., Pauliquevis, T., Maenhaut,

BGD
8, 1483–1527, 2011

W., Raes, N., Chi, X. G., Mayol-Bracero, O. L., Soto-Garcia, L. L., Claeys, M., Kourtchev, I., Rissler, J., Swietlicki, E., Tagliavini, E., Schkolnik, G., Falkovich, A. H., Rudich, Y., Fisch, G., and Gatti, L. V.: Overview of the inorganic and organic composition of size-segregated aerosol in Rondônia, Brazil, from the biomass-burning period to the onset of the wet season, J. Geophys. Res., 112, D01201, doi:10.1029/2005JD006741, 2007.

Gaudichet, A., Echalar, F., Chatenet, B., Quisefit, J. P., Malingre, G., Cachier, H., Buat-Menard, P., Artaxo, P., and Maenhaut, W.: Trace elements in tropical African savanna biomass burning aerosols, J. Atmos. Chem., 22, 19–39, 1995.

Generoso, S., Bey, I., Attié, J.-L., and Bréon, F.-M.: A satellite- and model-based assessment of the 2003 Russian fires: Impact on the Arctic region, J. Geophys. Res., 112, D15302, doi:10.1029/2006JD008344, 2007.

Giglio, L., van der Werf, G. R., Randerson, J. T., Collatz, G. J., and Kasibhatla, P.: Global estimation of burned area using MODIS active fire observations, Atmos. Chem. Phys., 6, 957–974, doi:10.5194/acp-6-957-2006, 2006.

Giglio, L., Randerson, J. T., van der Werf, G. R., Kasibhatla, P. S., Collatz, G. J., Morton, D. C., and DeFries, R. S.: Assessing variability and long-term trends in burned area by merging multiple satellite fire products, Biogeosciences, 7, 1171–1186, doi:10.5194/bg-7-1171-2010, 2010.

Gonzi, S. and Palmer, P. I.: Vertical transport of surface fire emissions observed from space, J. Geophys. Res., 115, D02306, doi:10.1029/2009JD012053, 2010.

Graham, B., Guyon, P., Maenhaut, W., Taylor, P. E., Ebert, M., Matthias-Maser, S., Mayol-Bracero, O. L., Godoi, R. H. M., Artaxo, P., Meixner, F. X., Moura, M. A., Rocha, C. H., Grieken, R. V., Glovsky, M. M., Flagan, R. C., and Andreae, M. O.: Composition and diurnal variability of the natural Amazonian aerosol, J. Geophys. Res., 108, 4765, doi:10.1029/2003JD004049, 2003.

Grégoire, J. M., Tansey, K., and Silva, J. M. N.: The GBA2000 initiative: developing a global burnt area database from SPOT-VEGETATION imagery, Int. J. Remote. Sens., 24, 1369–1376, doi:10.1080/0143116021000044850, 2003.

Guan, H., Esswein, R., Lopez, J., Bergstrom, R., Warnock, A., Follette-Cook, M., Fromm, M., and Iraci, L. T.: A multi-decadal history of biomass burning plume heights identified using aerosol index measurements, Atmos. Chem. Phys., 10, 6461–6469, doi:10.5194/acp-10-6461-2010, 2010.

Guieu, C., Bonnet, S., Wagener, T., and Loye-Pilot, M.-D: Biomass burning as a

source of dissolved iron to the open ocean?, Geophys. Res. Lett., 22, L19608, doi:10.1029/2005GL022962, 2005.
Hansen, M. C., DeFries, R. S., Townshend, J. R. G., Carroll, M., Dimiceli, C., and Sohlberg, R. A.: Global percent tree cover at a spatial resolution of 500 meters: First results of the MODIS vegetation continuous fields algorithm, Earth Interact., 7(10), 1–15, 2003.
Hansen, M. C., Stehman, V. S., and Potapov, P.: Quantification of global gross forest cover loss, P. Nat. Acad. Sci. USA, 107, 8650–8655, doi:10.1073/pnas.0912668107, 2010.
Heald, C. L., Jacob, D. J., Jones, D. B. A., Palmer, P. I., Logan, J. A., Streets, D. G., Sachse, G. W., Gille, J. C., Hoffman, R. N., and Nehrkorn, T.: Comparative inverse analysis of satellite (MOPITT) and aircraft (TRACE-P) observations to estimate Asian sources of carbon monoxide, J. Geophys. Res., 109, D23306, doi:10.1029/2004JD005185, 2004.
Hély, C., Caylor, K. K., Dowty, P., Alleaume, S., Swap, R. J., Shugart, H. H., and Justice, C. O.: A temporally explicit production efficiency model for fuel load allocation in southern Africa, Ecosystems, 10, 1116–1132, doi:10.1007/s10021-007-9082-3, 2007.
Hoelzemann, J. J., Schultz, M. G., Brasseur, G. P., Granier, C., and Simon, M.: The global wildland fire emission model GWEM: Evaluating the use of global area burnt data, J. Geophys. Res., 109, D14S04, doi:10.1029/2003JD003666, 2004.
Holloway, T., Levy, H., and Kasibhatla, P.: Global distribution of carbon monoxide, J. Geophys. Res., 105(D10), 12123–12147, 2000.
Huang, S., Siegert, F., Goldammer, J. G., and Sukhinin, A. I.: Satellite-derived 2003 wildfires in southern Siberia and their potential influence on carbon sequestration, Int. J. Rem. Sens., 30, 1479–1492, 2009.
Huete, A., Didan, K., Miura, T., Rodriguez, E. P., Gao, X., and Ferreira, L. G.: Overview of the radiometric and biophysical performance of the MODIS vegetation indices, Rem. Sens. Environ., 83, 195–213, 2002.
Hyer, E. J., Kasischke, E. S., and Allen, D. J.: Effects of source temporal resolution on transport simulations of boreal fire emissions, J. Geophys. Res., 112, D01302, doi:10.1029/2006JD007234, 2007.
Ito, A. and Feng, Y.: Role of dust alkalinity in acid mobilization of iron, Atmos. Chem. Phys., 10, 9237–9250, doi:10.5194/acp-10-9237-2010, 2010.
Ito, A. and Kawamiya, M.: Potential impact of ocean ecosystem changes due to global warming on marine organic carbon aerosols, Global Biogeochem. Cy., 24, GB1012, doi:10.1029/2009GB003559, 2010.

BGD
8, 1483–1527, 2011

Ito, A. and Penner, J. E.: Global estimates of biomass burning emissions based on satellite imagery for the year 2000, J. Geophys. Res., 109, D14S05, doi:10.1029/2003JD004423, 2004.
Ito, A. and Penner, J. E.: Estimates of CO emissions from open biomass burning in southern Africa for the year 2000, J. Geophys. Res., 110, D19306, doi:10.1029/2004JD005347, 2005.
Ito, A., Sillman, S., and Penner, J. E.: Effects of additional nonmethane volatile organic compounds, organic nitrates, and direct emissions of oxygenated organic species on global tropospheric chemistry, J. Geophys. Res., 112, D06309, doi:10.1029/2005JD006556, 2007a.
Ito, A., Ito, A., and Akimoto, H.: Seasonal and interannual variations in CO and BC emissions from open biomass burning in Southern Africa during 1998–2005, Global Biogeochem. Cy., 21, GB2011, doi:10.1029/2006GB002848, 2007b.
Ito, A., Sillman, S., and Penner, J. E.: Global chemical transport model study of ozone response to changes in chemical kinetics and biogenic volatile organic compounds emissions due to increasing temperatures: Sensitivities to isoprene nitrate chemistry and grid resolution, J. Geophys. Res., 114, D09301, doi:10.1029/2008JD011254, 2009.
Iwasaka, Y., Hiroaki, M., and Nagaya, K.: The transport and spatial scale of dust storm clouds: A case study of the dust storm event of April 1979, Tellus, Ser. B, 35, 189–196, 1983.
Jaffe, D., Bertschi, I., Jaeglé, L., Novelli, P., Reid, J. S., Tanimoto, H., Vingarzan, R., and Westphal, D. L.: Long-range transport of Siberian biomass burning emissions and impact on surface ozone in western North America, Geophys. Res. Lett., 31, L16106, doi:10.1029/2004GL020093, 2004.
Justice, C. O., Giglio, L., Korontzi, S., Owens, J., Morisette, J. T., Roy, D., Descloitres, J., Alleaume, S., Petitcolin, F., and Kaufman, Y.: The MODIS fire products, Remote Sens. Environ., 83, 244–262, 2002.
Kajii, Y., Kato, S., Streets, D. G., Tsai, N. Y., Shvidenko, A., Nilsson, S., McCallum, I., Minko, N. P., Abushenko, N., Altyntsev, D., and Khodzer, T. V.: Boreal forest fires in Siberia in 1998: Estimation of area burned and emissions of pollutants by advanced very high resolution radiometer satellite data, J. Geophys. Res., 107(D24), 4745, doi:10.1029/2001JD001078, 2002.
Kahn, R. A., Li, W.-H., Moroney, C., Diner, D. J., Martonchik, J. V., and Fishbein, E.: Aerosol source plume physical characteristics from space-based multiangle imaging, J. Geophys. Res., 112, D11205, doi:10.1029/2006JD007647, 2007.
Kahn, R. A., Chen, Y., Nelson, D. L., Leung, F.-Y., Li, Q., Diner, D. J., and Logan, J. A.: Wildfire

smoke injection heights: Two perspectives from space, Geophys. Res. Lett., 35, L04809, doi:10.1029/2007GL032165, 2008.

Kasischke, E. S. and Bruhwiler, L. P.: Emissions of carbon dioxide, carbon monoxide, and methane from boreal forest fires in 1998, J. Geophys. Res., 108(D1), 8146, doi:10.1029/2001JD000461, 2002.

Kasischke, E. S., Hyer, E. J., Novelli, P. C., Bruhwiler, L. P., French, N. H. F., Sukhinin, A. I., Hewson, J. H., and Stocks, B. J.: Influences of boreal fire emissions on Northern Hemisphere atmospheric carbon and carbon monoxide, Global Biogeochem. Cy., 19, GB1012, doi:10.1029/2004GB002300, 2005.

Kato, T., Ito, A., and Kawamiya, M.: Multiple temporal scale variability during the twentieth century in global carbon dynamics simulated by a coupled climate-terrestrial carbon cycle model, Clim. Dyn., 32, 901–923, doi:10.1007/s00382-009-0548-1, 2009.

Kovacs, K., Ranson, K. J., Sun, G., and Kharuk, V. I.: The relationship of the Terra MODIS fire product and anthropogenic features in the central Siberian landscape, Earth Interact., 8, 1–25, 2004.

Lamarque, J.-F., Bond, T. C., Eyring, V., Granier, C., Heil, A., Klimont, Z., Lee, D., Liousse, C., Mieville, A., Owen, B., Schultz, M. G., Shindell, D., Smith, S. J., Stehfest, E., Van Aardenne, J., Cooper, O. R., Kainuma, M., Mahowald, N., McConnell, J. R., Naik, V., Riahi, K., and van Vuuren, D. P.: Historical (1850-2000) gridded anthropogenic and biomass burning emissions of reactive gases and aerosols: methodology and application, Atmos. Chem. Phys., 10, 7017–7039, doi:10.5194/acp-10-7017-2010, 2010.

Langmann, B., Duncan, B., Textor, C., Trentmann, J., and van der Werf, G. R.: Vegetation fire emissions and their impact on air pollution and climate, Atmos. Environ., 43, 107–116, doi:10.1016/j.atmosenv.2008.09.047, 2009.

Lapina, K., Honrath, R. E., Owen, R. C., Martin, M. V., Hyer, E. J., and Fialho, P.: Late summer changes in burning conditions in the boreal regions and their implications for NO_x and CO emissions from boreal fires, J. Geophys. Res., 113, D11304, doi:10.1029/2007jd009421, 2008.

Lavoué, D., Liousse, C., Cachier, H., Stocks, B., and Goldammer, J.: Modeling of carbonaceous particles emitted by boreal and temperate wildfires at northern latitudes, J. Geophys. Res., 105(D22), 26871–26890, 2000.

Leung, F.-Y. T., Logan, J. A., Park, R., Hyer, E., Kasischke, E., Streets, D., and Yurganov, L.: Impacts of enhanced biomass burning in the boreal forests in 1998 on tropospheric chemistry

and the sensitivity of model results to the injection height of emissions, J. Geophys. Res., 112, D10313, doi:10.1029/2006JD008132, 2007.
Liu, X., Penner, J. E., and Herzog, M.: Global modeling of aerosol dynamics: Model description, evaluation and interactions between sulfate and non-sulfate aerosols, J. Geophys. Res., 110, D18206, doi:10.1029/2004JD005674, 2005.
Luo, C., Mahowald, N., Bond, T., Chuang, P. Y., Artaxo, P., Siefert, R., Chen, Y., and Schauer, J.: Combustion iron distribution and deposition, Global Biogeochem. Cy., 22, GB1012, doi:10.1029/2007GB002964, 2008.
Maher, B. A., Prospero, J. M., Mackie, D., Gaiero, D., Hesse, P. P., and Balkanski, Y.: Global connections between aeolian dust, climate and ocean biogeochemistry at the present day and at the last glacial maximum, Earth Sci. Rev., 99, 61–97, 2010.
Mahowald, N. M., Sebastian, E., Luo, C., Sealy, A., Artaxo, P., Benitez-Nelson, C., Bonnet, S., Chen, Y., Chuang, P. Y., Cohen, D. D., Dulac, F., Herut, B., Johansen, A. M., Kubilay, N., Losno, R., Maenhaut, W., Paytan, A., Prospero, J. M., Shank, L. M., and Siefert, R. L.: Atmospheric iron deposition: global distribution, variability, and human perturbations, Annu. Rev. Mar. Sci., 1, 245–278, 2009.
Marlon, J. R., Bartlein, P. J., Carcaillet, C., Gavin, D. G., Harrison, S. P., Higuera, P. E., Joos, F., Power, M. J., and Prentice, I. C.: Climate and human influences on global biomass burning over the past two millennia, Nature Geosci., 1, 697–702, doi:10.1038/ngeo313, 2008.
Martin, J. H.: Glacial-interglacial CO_2 change: The iron hypothesis, Paleoceanography, 5, 1–13, doi:10.1029/PA005i001p00001, 1990.
Martin, J. H., Coale, K. H., Johnson, K. S., Fitzwater, S. E., Gordon, R. M., Tanner, S. J. Hunter, C. N., Elrod, V. A., Nowicki, J. L., Coley, T. L., Barber, R. T., Lindley, S., Watson, A. J., Vanscoy, K., Law, C. S., Liddicoat, M. I., Ling, R., Stanton, T., Stockel, J., Collins, C., Anderson, A., Bidigare, R., Ondrusek, M., Latasa, M., Millero, F. J., Lee, K., Yao, W., Zhang, J. Z., Friederich, G., Sakamoto, C., Chavez, F., Buck, K., Kolber, Z., Greene, R., Falkowski, P., Chisholm, S. W., Hoge, F., Swift, R., Yungel, J., Turner, S., Nightingale, P., Hatton, A., Liss, P., and Tindale, N. W.: Testing the iron hypothesis in ecosystems of the equatorial Pacific Ocean, Nature, 371, 123–129, 1994.
Mills, M. M., Ridame, C., Davey, M., La Roche, J., and Geider, R. J.: Iron and phosphorus co-limit nitrogen fixation in the eastern tropical north Atlantic, Nature, 429, 292–294, 2004.
Nelson, D., Lawshe, C., Mazzoni, D., Diner, D., and Kahn, R.: MISR Plume Height Project: Suggestion for using data, Jet Propulsion Lab, NASA, available at: http://www-misr2.jpl.

BGD
8, 1483–1527, 2011

nasa.gov/EPA-Plumes/suggestions4UsingData.cfm (last access: 16 February 2011), 2008.
New, M., Hulme, M., and Jones, P.: Representing twentieth-century space-time climate variability, Part II: Development of 1901–1996 monthly grids of terrestrial surface climate, J. Clim., 13(13), 2217–2238, 2000.
O'Dowd, C. D., Facchini, M. C., Cavalli, F., Ceburnis, D., Mircea, M., Decesari, S., Fuzzi, S., Yoon, Y. J., and Putaud, J.-P.: Biogenically driven organic contribution to marine aerosol, Nature, 431, 676–680, 2004.
Penner, J. E., Haselman Jr., L. C., and Edwards, L. L.: Smoke-plume distribution above large-scale fires: Implications for simulations of "Nuclear Winter", J. Clim. Appl. Meteorol., 25, 1434–1444, 1986.
Paris, R., Desboeufs, K. V., Formenti, P., Nava, S., and Chou, C.: Chemical characterisation of iron in dust and biomass burning aerosols during AMMA-SOP0/DABEX: implication for iron solubility, Atmos. Chem. Phys., 10, 4273–4282, doi:10.5194/acp-10-4273-2010, 2010.
Pétron, G., Granier, C., Khattatov, B., Yudin, V., Lamarque, J.-F., Emmons, L., Gille, J., and Edwards, D. P.: Monthly CO surface sources inventory based on the 2000–2001 MOPITT satellite data, Geophys. Res. Lett., 31, L21107, doi:10.1029/2004GL020560, 2004.
Potapov, P., Hansen, M. C., Stehman, S. V., Loveland, T. R., and Pittman, K.: Combining MODIS and Landsat imagery to estimate and map boreal forest cover loss, Rem. Sens. Environ., 112(9), 3708–3719, 2008.
Potapov, P., Hansen, M. C., Stehman, S. V., Pittman, K., and Turubanova, S.: Gross forest cover loss in temperate forests: Biome-wide monitoring results using MODIS and Landsat data, J. Appl. Rem. Sens., 3, 1–23, doi:10.1117/1.3283904, 2009.
Pfister, G., Hess, P. G., Emmons, L. K., Lamarque, J.-F., Wiedinmyer, C., Edwards, D. P., Pétron, G., Gille, J. C., and Sachse, G. W.: Quantifying CO emissions from the 2004 Alaskan wildfires using MOPITT CO data, Geophys. Res. Lett., 32, L11809, doi:10.1029/2005GL022995, 2005.
Reid, J. S., Koppmann, R., Eck, T. F., and Eleuterio, D. P.: A review of biomass burning emissions part II: intensive physical properties of biomass burning particles, Atmos. Chem. Phys., 5, 799–825, doi:10.5194/acp-5-799-2005, 2005.
Rotman, D. A., Atherton, C. S., Bergmann, D. J., Cameron-Smith, P. J., Chuang, C. C., Connell, P. S., Dignon, J. E., Franz, A., Grant, K. E., Kinnison, D. E., Molenkamp, C. R., Proctor, D. D., and Tannahill, J. R.: IMPACT, the LLNL 3-D global atmospheric chemical transport model for the combined troposphere and stratosphere: Model description and analysis of ozone and

other trace gases, J. Geophys. Res., 109, D04303, doi:10.1029/2002JD003155, 2004.
Roy, D. P., Boschetti, L., Justice, C. O., and Ju, J.: The collection 5 MODIS burned area product – Global evaluation by comparison with the MODIS active fire product, Rem. Sens. Environ., 112, 3690–3707, 2008.
Sato, H., Itoh, A., and Kohyama, T.: SEIB-DGVM: a new dynamic global vegetation model using a spatially explicit individual-based approach, Ecol. Model., 200, 279–307, 2007.
Sato, H., Kobayashi, H., and Delbart, N.: Simulation study of the vegetation structure and function in eastern Siberian larch forests using the individual-based vegetation model SEIB-DGVM, For. Ecol. Manage., 259, 301–311, doi:10.1016/j.foreco.2009.10.019, 2010.
Schroth, A. W., Crusius, J., Sholkovitz, E. R., and Bostick, B. C.: Iron solubility driven by speciation in dust sources to the ocean, Nat. Geosci., 2, 337–340, doi:10.1038/ngeo501, 2009.
Schultz, M. and Rast, S.: Emission datasets and methodologies for estimating emissions, available at: http://retro.enes.org (last access: 16 February 2011), RETRO Report D1-6, 2007.
Sedwick, P. N., Sholkovitz, E. R., and Church, T. M.: Impact of anthropogenic combustion emissions on the fractional solubility of aerosol iron: Evidence from the Sargasso Sea, Geochem. Geophys. Geosyst., 8, Q10Q06, doi:10.1029/2007GC001586, 2007.
Seiler, W. and Crutzen, P. J.: Estimates of gross and net fluxes of carbon between the biosphere and the atmosphere from biomass burning, Clim. Change, 2, 207–247, 1980.
Shindell, D. T., Faluvegi, G., Stevenson, D. S., Krol, M. C., Emmons, L. K., Lamarque, J. F., Petron, G., Dentener, F. J., Ellingsen, K., Schultz, M. G., Wild, O., Amann, M., Atherton, C. S., Bergmann, D. J., Bey, I., Butler, T., Cofala, J., Collins, W. J., Derwent, R. G., Doherty, R. M., Drevet, J., Eskes, H. J., Fiore, A. M., Gauss, M., Hauglustaine, D. A., Horowitz, L.W., Isaksen, I. S. A., Lawrence, M. G., Montanaro, V., Muller, J. F., Pitari, G., Prather, M. J., Pyle, J. A., Rast, S., Rodriguez, J. M., Sanderson, M. G., Savage, N. H., Strahan, S. E., Sudo, K., Szopa, S., Unger, N., van Noije, T. P. C., and Zeng, G.: Multimodel simulations of carbon monoxide: Comparison with observations and projected near-future changes, J. Geophys. Res., 111, D19306, doi:10.1029/2006JD007100, 2006.
Sholkovitz, E. R., Sedwick, P. N., and Church, T. M.: Influence of anthropogenic combustion emissions on the deposition of soluble aerosol iron to the ocean: Empirical estimates for island sites in the North Atlantic, Geochim. Cosmochim. Acta, 73, 3981–4003, 2009.
Simon, M., Plummer, S., Fierens, F., Hoelzemann, J. J., and Arino, O.: Burnt area detection at global scale using ATSR-2: The GLOBSCAR products and their qualification, J. Geophys.

BGD
8, 1483–1527, 2011

Res., 109, D14S02, doi:10.1029/2003JD003622, 2004.
Soja, A. J., Cofer, W. R., Shugart, H. H., Sukhinin, A. I., Stackhouse, P. W., McRae, D. J., and Conard, S. G.: Estimating fire emissions and disparities in boreal Siberia (1998–2002), J. Geophys. Res., 109, D14S06, doi:10.1029/2004JD004570, 2004.
Tanimoto, H., Kajii, Y., Hirokawa, J., Akimoto, H., and Minko, N. P.: The atmospheric impact of boreal forest fires in far eastern Siberia on the seasonal variation of carbon monoxide: observations at Rishiri, a northern remote island in Japan, Geophys. Res. Lett., 27, 4073–4076, 2000.
Textor, C., Schulz, M., Guibert, S., Kinne, S., Balkanski, Y., Bauer, S., Berntsen, T., Berglen, T., Boucher, O., Chin, M., Dentener, F., Diehl, T., Feichter, J., Fillmore, D., Ginoux, P., Gong, S., Grini, A., Hendricks, J., Horowitz, L., Huang, P., Isaksen, I. S. A., Iversen, T., Kloster, S., Koch, D., Kirkevåg, A., Kristjansson, J. E., Krol, M., Lauer, A., Lamarque, J. F., Liu, X., Montanaro, V., Myhre, G., Penner, J. E., Pitari, G., Reddy, M. S., Seland, Ø., Stier, P., Takemura, T., and Tie, X.: The effect of harmonized emissions on aerosol properties in global models - an AeroCom experiment, Atmos. Chem. Phys., 7, 4489–4501, doi:10.5194/acp-7-4489-2007, 2007.
Thonicke, K., Venevsky, S., Sitch, S., and Cramer, W.: The role of fire disturbance for global vegetation dynamics: coupling fire into a Dynamic Global Vegetation Model, Global Ecol. Biogeogr., 10, 661–678, doi:10.1046/j.1466-822X.2001.00175.x, 2001.
Trentmann, J., Luderer, G., Winterrath, T., Fromm, M. D., Servranckx, R., Textor, C., Herzog, M., Graf, H.-F., and Andreae, M. O.: Modeling of biomass smoke injection into the lower stratosphere by a large forest fire (Part I): reference simulation, Atmos. Chem. Phys., 6, 5247–5260, doi:10.5194/acp-6-5247-2006, 2006.
Tsuda, A., Takeda, S., Saito, H., Nishioka, J., Nojiri, Y., Kudo, I., Kiyosawa, H., Shiomoto, A., Imai, K., Ono, T., Shimamoto, A., Tsumune, D., Yoshimura, T., Aono, T., Hinuma, A., Kinugasa, M., Suzuki, K., Sohrin, Y., Noiri, Y., Tani, H., Deguchi, Y., Tsurushima, N., Ogawa, H., Fukami, K., Kuma, K., and Saino, T.: A mesoscale iron enrichment in the western Subarctic Pacific induces a large centric diatom bloom, Science, 300, 958–961, 2003.
Turetsky, M. R., Kane, E. S., Harden, J. W., Ottmar, R. D., Manies, K. L., Hoy, E., and Kasischke, E. S.: Recent acceleration of biomass burning and carbon losses in Alaskan forests and peatlands, Nature Geosci., 5, 27–31, doi:10.1038/ngeo1027, 2011.
Turquety, S., Logan, J. A., Jacob, D. J., Hudman, R. C., Leung, F-Y., Heald, C. L., Yantosca, M., Wu, S., Emmons, L. K., Edwards, D. P., and Sachse, G. W.: Inventory of boreal fire emis-

BGD
8, 1483–1527, 2011

sions for North America in 2004: Importance of peat burning and pyroconvective injection, J. Geophys. Res., 112, D12S03, doi:10.1029/2006JD007281, 2007.
Uematsu, M., Duce, R. A., Prospero, J. M., Chen, L., Merrill, J. T., and McDonald, R. L.: Transport of mineral aerosol from Asia over the North Pacific Ocean, J. Geophys. Res., 88, 5343–5352, 1983.
Val Martin, M., Logan, J. A., Kahn, R. A., Leung, F.-Y., Nelson, D. L., and Diner, D. J.: Smoke injection heights from fires in North America: analysis of 5 years of satellite observations, Atmos. Chem. Phys., 10, 1491–1510, doi:10.5194/acp-10-1491-2010, 2010.
van der Werf, G. R., Randerson, J. T., Collatz, G. J., and Giglio, L.: Carbon emissions from fires in tropical and subtropical ecosystems, Global Change Biol., 9, 547–562, 2003.
van der Werf, G. R., Morton, D. C., DeFries, R. S., Giglio, L., Randerson, J. T., Collatz, G. J., and Kasibhatla, P. S.: Estimates of fire emissions from an active deforestation region in the southern Amazon based on satellite data and biogeochemical modelling, Biogeosciences, 6, 235–249, doi:10.5194/bg-6-235-2009, 2009.
van der Werf, G. R., Randerson, J. T., Giglio, L., Collatz, G. J., Mu, M., Kasibhatla, P. S., Morton, D. C., DeFries, R. S., Jin, Y., and van Leeuwen, T. T.: Global fire emissions and the contribution of deforestation, savanna, forest, agricultural, and peat fires (1997-2009), Atmos. Chem. Phys., 10, 11707–11735, doi:10.5194/acp-10-11707-2010, 2010.
Van Vuuren, D. P., Edmonds, J., Thomson, A., Riahi, K., Kainuma, M., Matsui, T., Hurtt, G. C., Lamarque, J.-F., Meinshausen, M., Smith, S., Granier, C., Rose, S. K., and Hibbard, K. A.: Representative Concentration Pathways: An overview, Clim. Change, submitted, 2010.
Wang, Z., Chappellaz, J., Park, K., and Mak, J. E.: Large variations in southern hemisphere biomass burning during the last 650 years, Science, 330, 1663–1666, 2010.
Yurganov, L. N., Duchatelet, P., Dzhola, A. V., Edwards, D. P., Hase, F., Kramer, I., Mahieu, E., Mellqvist, J., Notholt, J., Novelli, P. C., Röckmann, A., Scheel, H. E., Schneider, M., Schulz, A., Strandberg, A., Sussmann, R., Tanimoto, H., Velazco, V., Drummond, J. R., and Gille, J. C.: Increased Northern Hemispheric carbon monoxide burden in the troposphere in 2002 and 2003 detected from the ground and from space, Atmos. Chem. Phys., 5, 563–573, doi:10.5194/acp-5-563-2005, 2005.
Zhang, Y.-H., Wooster, M. J., Tutubalina, O., and Perry, G. L. W.: Monthly burned area and forest fire carbon emission estimates for the Russian Federation from SPOT VGT, Rem. Sens. Environ., 87, 1–15, 2003.

BGD
8, 1483–1527, 2011

Table 1. Combustion factor of ground layer organic matter as a function of fire severity and fuel conditions during the fire season used for emission estimations based on Kasischke et al. (2005).

	Wet	Middle	Dry
Low severity			
Surface	0.08	0.15	0.31
Crown	0.12	0.23	0.50
High severity			
Surface	0.15	0.31	0.62
Crown	0.23	0.46	1.00

BGD
8, 1483–1527, 2011

Table 2. Annual amounts of burned areas and biomass burning emissions in the high latitude Northern Hemisphere (> 30° N latitude) from 2001 to 2005.

Year	Total BA[a]	Forested BA[a]	CO[b]	NO[c]	$PM_{2.5}$[d]
2001	256	13	13	0.17	1.3
2002	331	38	56	0.64	5.6
2003	480	51	82	0.92	8.1
2004	364	33	33	0.36	3.3
2005	332	22	32	0.35	3.1

[a] Burned areas (10^3 km^2 yr^{-1})
[b] CO emissions (Tg CO yr^{-1})
[c] NO emissions (Tg NO yr^{-1})
[d] $PM_{2.5}$ emissions (Tg $PM_{2.5}$ yr^{-1})

BGD
8, 1483–1527, 2011

Table 3. Modeled (Exp 1–4) and observed monthly averaged total column of CO ($\times 10^{18}$ molecules cm^{-2}) in eastern Siberia (40°–70° N; 100°–140° E) (mean ± standard deviation).

	MOPITT	Exp 1	Exp 2	Exp 3	Exp 4
Horizontal resolution		4° × 5°	4° × 5°	2° × 2.5°	1° × 1°
Temporal resolution		Monthly	Daily	Daily	Daily
Injection height		Surface	MISR[a]	MISR[a]	MISR[a]
August 2002	2.3 ± 0.2	1.8 ± 0.1	1.8 ± 0.1	2.0 ± 0.1	2.0 ± 0.1
May 2003	2.8 ± 0.4	2.2 ± 0.3	2.2 ± 0.3	2.3 ± 0.3	2.3 ± 0.3

[a] Satellite-derived plume height from MISR is used for the injection height of a smoke plume.

BGD
8, 1483–1527, 2011

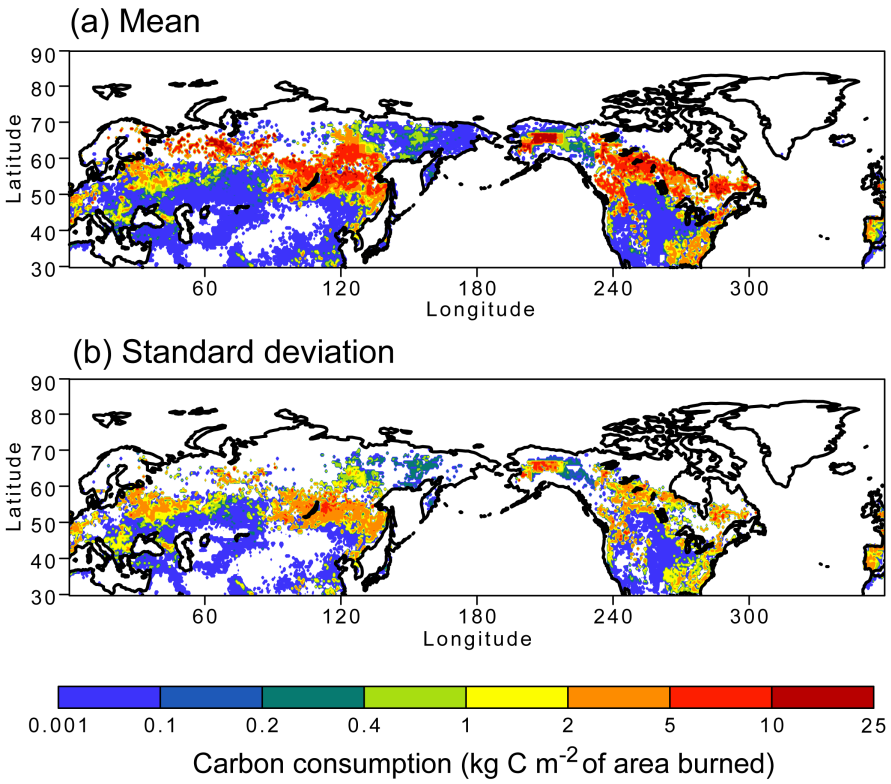

Fig. 1. Carbon consumption estimates (kg C m^{-2} of area burned) **(a)** 5-year means over 2001–2005 and **(b)** standard deviations.

BGD
8, 1483–1527, 2011

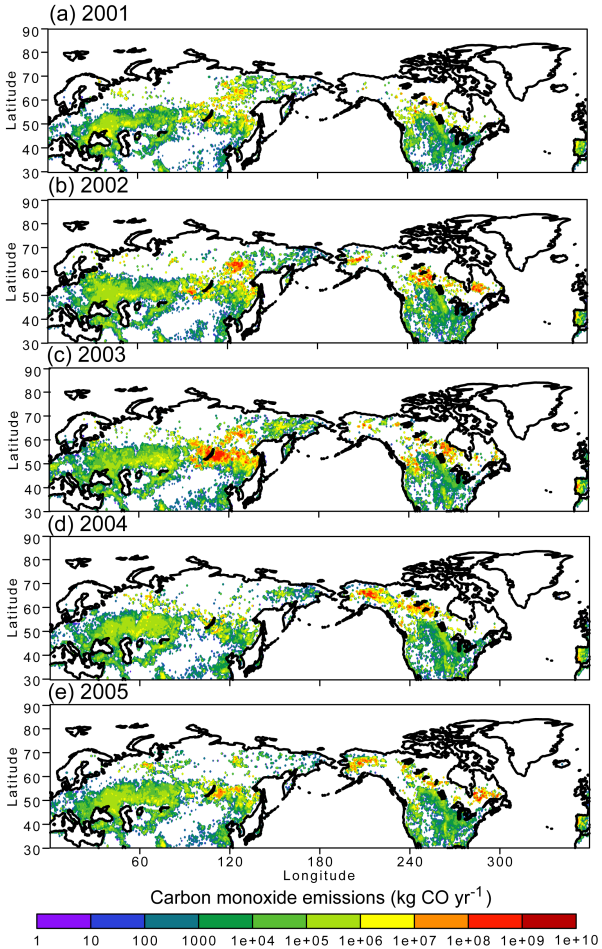

Fig. 2. CO emissions (kg CO yr^{-1}) over the high latitude Northern Hemisphere in **(a)** 2001, **(b)** 2002, **(c)** 2003, **(d)** 2004, and **(e)** 2005.

BGD
8, 1483–1527, 2011

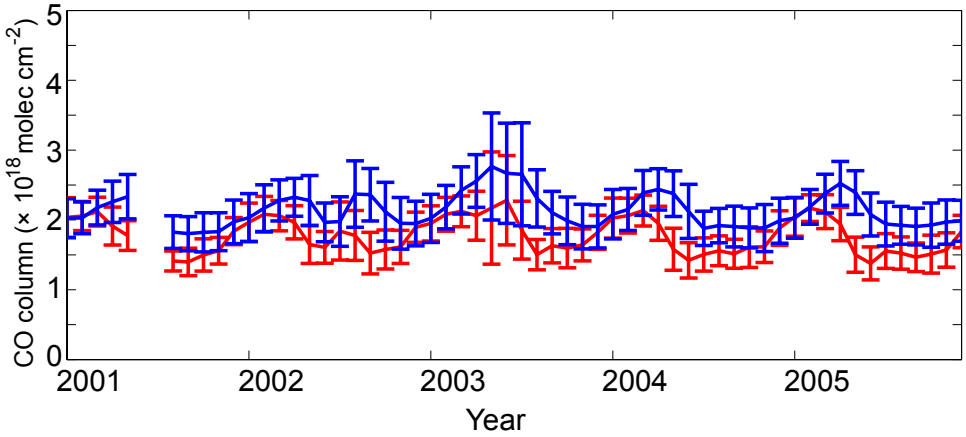

Fig. 3. Modeled (red) and observed (blue) monthly averaged total column of CO ($\times 10^{18}$ molecules cm^{-2}) over eastern Siberian region (40°–70° N; 100°–140° E) during 2001–2005.

BGD
8, 1483–1527, 2011

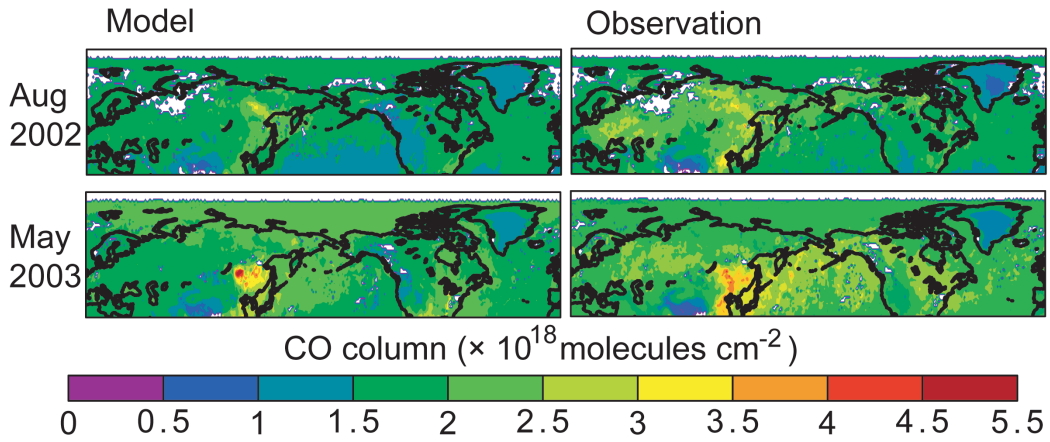

Fig. 4. Comparison of monthly averaged total column of CO ($\times 10^{18}$ molecules cm^{-2}) between model results and observations in August 2002 and May 2003.

BGD
8, 1483–1527, 2011

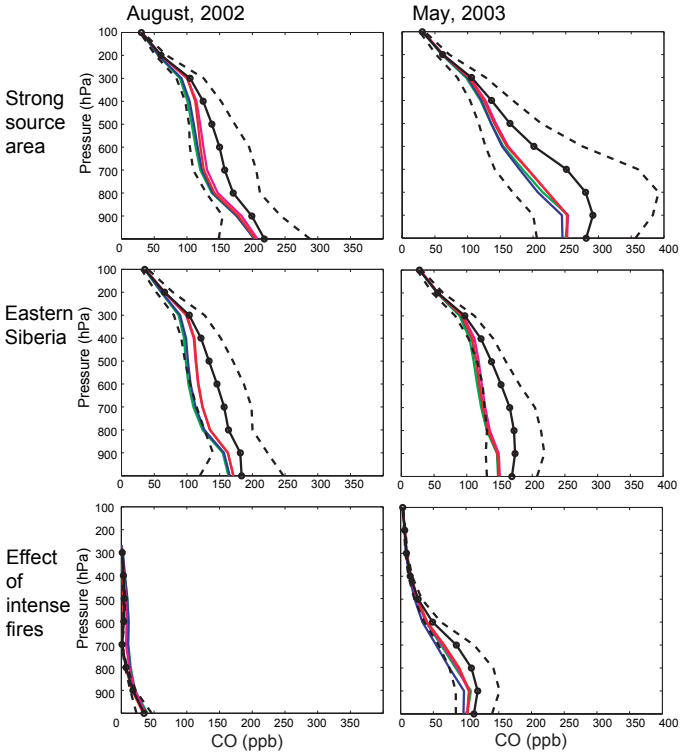

Fig. 5. Comparison of CO (ppb) between model results from different simulations and observations over strong source areas and eastern Siberian region excluding the strong source areas in August 2002 and May 2003. The differences in CO between the strong source areas and other areas in eastern Siberian region are also shown. The black circles represent the average of measurements over the selected regions and the periods of clear-sky days during daytime MOPITT overpasses. The dashed lines show the standard deviations of daily measured values. The different colors correspond to different experiments; green (Exp 1), blue (Exp 2), magenta (Exp 3), and red (Exp 4).

BGD
8, 1483–1527, 2011

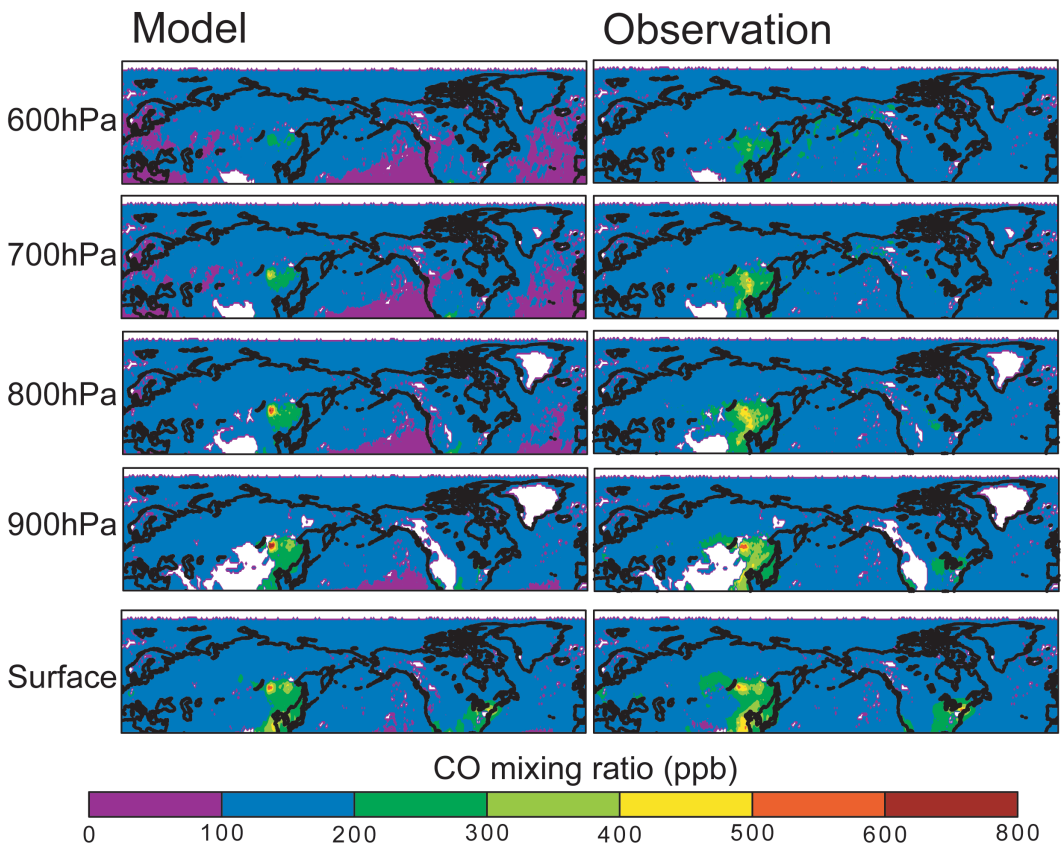

Fig. 6. Comparison of CO mixing ratio in ppb between model results and observations in May 2003 at five pressure layers (surface, 900 hPa, 800 hPa, 700 hPa, and 600 hPa).

BGD
8, 1483–1527, 2011

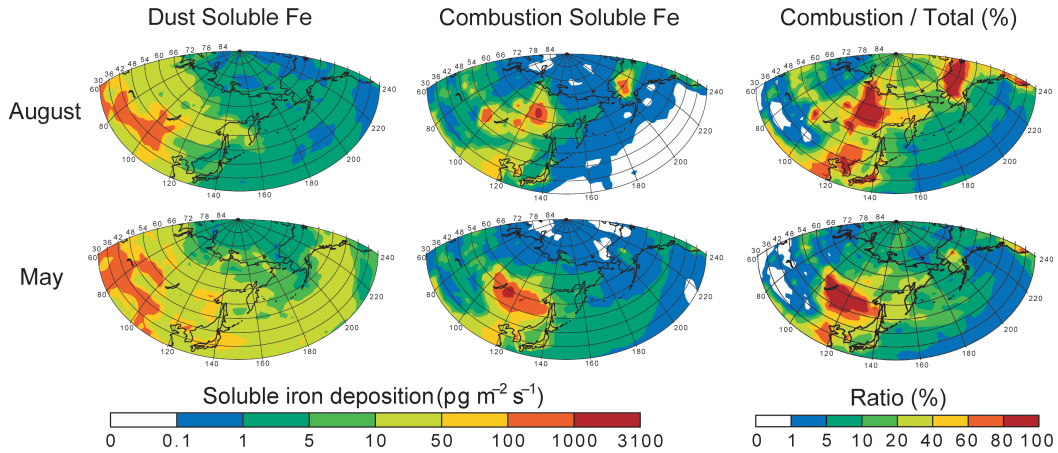

Fig. 7. Comparison of monthly averaged soluble iron deposition (pg m^{-2} s^{-1}) to the ocean from dust and combustion (Exp 5) sources in August and May. The percentage of the total deposited soluble iron which comes from combustion is also shown.

BGD
8, 1483–1527, 2011

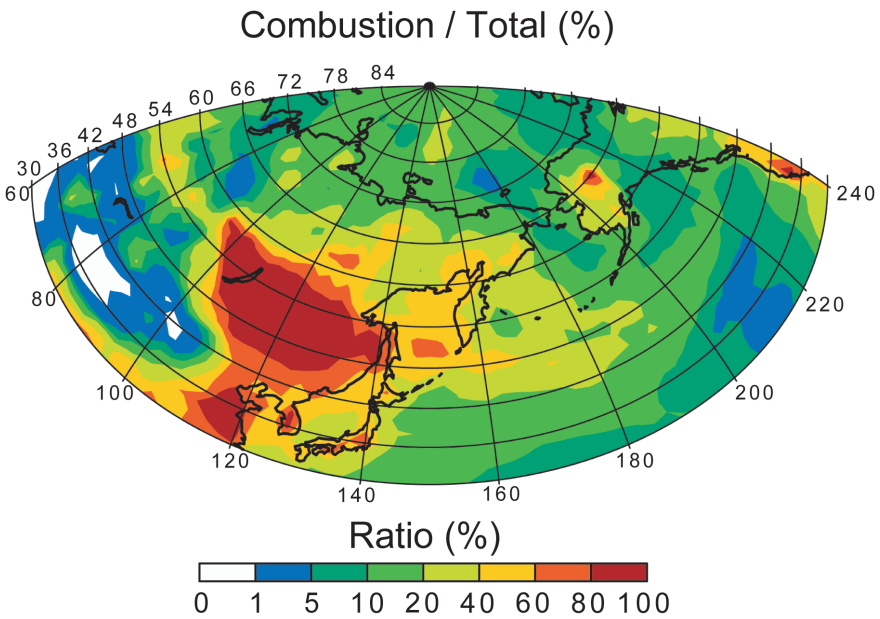

Fig. 8. Ratio of the deposited soluble iron from combustion (Exp 5) to total deposition, which is the sum of combustion and dust sources without the atmospheric processing by acidic species.

BGD
8, 1483–1527, 2011